AAS 23-268

BASELINE ORBIT GENERATION FOR NEAR RECTILINEAR HALO ORBITS

Emily M. Zimovan-Spreen[*], Stephen T. Scheuerle[†], Brian P. McCarthy[‡], Diane C. Davis[§], and Kathleen C. Howell[¶]

A Near Rectilinear Halo Orbit (NRHO) with an eclipse-favorable phase serves as the current baseline orbit for the Gateway mission. The baseline provides a catalog of orbit maintenance targets and serves as a reference path for other types of trajectory analysis. In this investigation, an automated multiple-shooting differential corrections strategy is developed to generate many-revolution, long-duration, ballistic baseline orbits in a higher-fidelity ephemeris force model at the eclipse-avoidant phases and at other alternative phases. Additional geometric considerations for eclipse avoidance in the NRHO are presented and utilized within a long-lead orbit maintenance-based phase shift strategy.

INTRODUCTION

Expanding human spaceflight beyond low Earth orbit, the Gateway[1] will serve as both a proving ground for deep space technologies and a staging location for missions to the lunar surface and beyond. The planned operational orbit for the Gateway is an Earth-Moon L2 Near Rectilinear Halo Orbit (NRHO) in a 9:2 lunar synodic resonance with the Moon.[2] This orbit satisfies many mission objectives and constraints, including low orbit maintenance cost and limited passages through the shadows of the Earth and Moon. The nominal orbit maintenance algorithm utilizes targets from a baseline trajectory; the operational trajectory will be maintained nearby this baseline.[3] Thus, a baseline trajectory spanning the Gateway lifetime is necessary for orbit maintenance propellant cost predictions and other operational investigations.

The current Gateway baseline NRHO, available on the JPL NAIF server, is carefully aligned in phase to avoid long eclipses from the Earth's shadow.[2,4] This baseline, originally generated in 2017 and denoted here as the "2017 baseline," has a start epoch in January 2020. Gateway operations are expected to begin in 2025 with the delivery of the co-manifested vehicle (CMV), which includes the Habitation and Logistics Outpost (HALO) and the Power and Propulsion Element (PPE). As the current baseline orbit extends through 2035, the generation of a new baseline that also satisfies operational constraints (e.g., Earth eclipse avoidance) is necessary to encompass the full 15-year mission lifetime. To construct the new baseline for the 15-year mission, this investigation leverages information about the Sun-Earth-Moon geometry to inform when the path of the spacecraft within the NRHO passes through the shadow of the Earth. The original 2017 baseline achieved its eclipse-favorable phase via a time-intensive process requiring significant human interaction. This investigate outlines an automated approach to generate eclipse-favorable NRHO baseline trajectories spanning 15+ years in duration. A process to incorporate spherical harmonics of the Moon is detailed.

Over the course of Gateway's lifetime, excursions to and from Gateway may require rephasing of spacecraft within the NRHO. That is, to enable mission opportunities or facilitate rendezvous with a visiting vehicle, it may be desirable to temporarily change the phase within the 9:2 NRHO. In such a scenario, a plan for

[*]Gateway Mission Design Engineer, Flight Mechanics and Trajectory Design Branch, NASA Johnson Space Center, emily.m.spreen@nasa.gov
[†]Ph.D. Candidate, School of Aeronautics and Astronautics, Purdue University, sscheuer@purdue.edu
[‡]Gateway Mission Design Engineer, a.i. solutions, Inc., brian.mccarthy@ai-solutions.com
[§]Gateaway Mission Design Lead, Flgith Mechanics and Trajectory Design Branch, NASA Johnson Space Center, diane.c.davis@nasa.gov
[¶]Hsu Lo Distinguished Professor of Aeronautics and Astronautics, Purdue University, howell@purdue.edu

the phase change must be in place well in advance of the rendezvous. Thus, a long-lead phase change could be executed over the course of weeks or months. However, techniques often applied in low Earth or low lunar orbit are not applicable for operations in the NRHO due to multi-body gravitational effects. A preliminary investigation into strategies for long-lead phase changes (e.g., those used for rendezvous or alternative mission opportunities) suggest low-cost methods exist to rephase the Gateway.[5] A long-lead phase change strategy that employs modified targets, or targets derived from alternative baseline trajectories, within the orbit maintenance (OM) algorithm can be used to adjust the phase of Gateway over the course of many revolutions. Geometric considerations can be used to change phase while avoiding passage through Earth's shadow. The current investigation continues the development of long-lead rephasing strategies for spacecraft within the NRHO and presents a geometry-based algorithm to avoid long-duration eclipsing in off-nominal or phase-shifted NRHOs. Shorter-lead phase change strategies, investigated by McCarthy et al., offer options to more rapidly transfer between phases of the NRHO.[6]

BACKGROUND

Dynamical Models

The Circular Restricted 3-Body Problem The Circular Restricted 3-Body Problem, abbreviated as CR3BP, serves as a reasonable approximation to higher-fidelity dynamical models in the Earth-Moon system while offering simplifications that allow for more straightforward concept development. Within this application of the CR3BP, the motion of a massless spacecraft under the gravitational influence of two primary bodies, P_1, the Earth, and P_2, the Moon, is considered. These two primary bodies, modeled as point masses, are assumed to move in circular orbits about their common barycenter, B. The motion of the spacecraft is then described relative to a coordinate frame, $\hat{x}$-$\hat{y}$-$\hat{z}$, that rotates with the motion of the Earth and Moon. In the Earth-Moon rotating frame, the location of the spacecraft is described by the vector $\mathbf{r}_{B/sc}$, originating at the barycenter, and is defined by the coordinates (x, y, z). By convention, quantities in the CR3BP are nondimensionalized such that the Earth-Moon distance, as well as the mean motion of the primaries, are both equal to a constant value of unity. As a consequence of the nondimensionalization, the distances from the Earth and Moon to the barycenter are represented as $1-\mu$ and μ, respectively, where the parameter μ equals the ratio of the mass of the Moon to the total mass of the system; in this case, $\mu = 0.01215$. Within the context of the rotating frame, the scalar equations of motion for the spacecraft are

$$\ddot{x} - 2\dot{y} = \frac{\partial U}{\partial x},\ \ddot{y} + 2\dot{x} = \frac{\partial U}{\partial y},\ \ddot{z} = \frac{\partial U}{\partial z} \tag{1}$$

where the pseudo-potential function, $U = \frac{1}{2}(x^2+y^2) + \frac{1-\mu}{d} + \frac{\mu}{r}$. The values for d and r within the pseudo-potential function are define as $d = \sqrt{(x+\mu)^2+y^2+z^2}$, and $r = \sqrt{(x-1+\mu)^2+y^2+z^2}$.

The N-Body Ephemeris Model For higher-fidelity analysis of behavior within the NRHO, N-body differential equations and planetary ephemerides are employed. In the ephemeris model, the motion of the particle of interest (e.g., a spacecraft), P_i, is rendered relative to a central body, P_q, in an inertial frame described in terms of the coordinates $\hat{X}$-$\hat{Y}$-$\hat{Z}$. The well-known dimensional N-body relative vector equation of motion is written as

$$\ddot{\mathbf{r}}_{qi} = -G\frac{(m_i+m_q)}{r_{qi}^3}\mathbf{r}_{qi} + G\sum_{\substack{j=1 \\ j\neq i,q}}^{N} m_j\left(\frac{\mathbf{r}_{ij}}{r_{ij}^3} - \frac{\mathbf{r}_{qj}}{r_{qj}^3}\right) \tag{2}$$

where G denotes the universal gravitational constant, $m_{(\cdot)}$ is the mass of $P_{(\cdot)}$, and the vector quantity $\mathbf{r}_{[a][b]}$ denotes the vector from body $[a]$ to body $[b]$. Within this analysis, the relative position of each perturbing body with respect to the central body is instantaneously computed by employing NAIF SPICE ephemeris data. The Moon is selected as the central body for numerical integration in the J2000 inertial frame. Initially, solar system bodies are included as point masses. Additional fidelity in the baseline NRHO is offered by modeling the Moon's gravity using the GRAIL model (GRGM660PRIM) truncated to degree and order 8. Expansion to a 16 by 16 model is included, as well. All spherical harmonics are added to the baseline using FreeFlyer Astrodynamics Software.[7]

For orbit maintenance analysis, solar radiation pressure (SRP) acting on a sphere with an area to mass ratio of 0.02 is included in the force model. Operational errors on the spacecraft are also considered. In these simulations, each OMM is associated with a navigation error on the spacecraft state of 1 km in position and 1 cm/s in velocity. Maneuver execution errors are comprised of three components: 1.5% proportional, 1 degree pointing, and 1.42 mm/s fixed, and are applied to each OM maneuver. Mismodeling in solar radiation pressure (SRP) assumptions provide 15% error in area and 30% error in coefficient of reflectivity. Momentum wheel desaturations are assumed to occur one time per revolution near perilune with a translational ΔV component of 1 cm/s applied in a random direction. All values are 3σ and are implemented as Gaussian errors with zero mean.

Orbit Maintenance Algorithm

The nominal Gateway orbit maintenance algorithm is designed to achieve a particular perilune passage time, or phase, as well as maintain the geometry of the NRHO. Maneuvers are placed along each revolution at a true anomaly of TA = 200°, about one day prior to perilune passage. A differential corrector is employed to initially design a maneuver that delivers a downstream velocity that is targeted to meet the constraint at a subsequent perilune passage, i.e.,

$$v_x = v_{xref} \pm v_{tol} \tag{3}$$

where v_x is the x-component of the rotating velocity at the controlled spacecraft's perilune passage in the Earth-Moon rotating frame at some target horizon downstream, v_{xref} is the x-component of rotating velocity along a baseline NRHO at its respective perilune passage, and the tolerance v_{tol} is nominally set to 0.45 m/s. The targeting horizon is initially set to 6.2 revolutions, so that the rotating x-velocity constraint in Equation 3 is satisfied at the seventh perilune passage downstream from the maneuver. If the targeter fails to converge, the targeting horizon is reduced successively until convergence is achieved. The resulting Δv is used as an initial guess to subsequently target both v_x and a weighted perilune passage time from the reference. The weighting is implemented by defining a target epoch

$$t_{targ} = W_t \left(t_{pref} - t_p\right) + t_p \tag{4}$$

where W_t is an empirically selected weighting factor, t_{pref} is the perilune passage time along a baseline NRHO, and t_p is the perilune passage time achieved by the maintained spacecraft after each iteration. Within the differential corrections algorithm, the weighted perilune passage time, t_{targ}, is achieved to within tolerance, i.e.,

$$t_p = t_{targ} \pm t_{tol} \tag{5}$$

where t_{tol} is nominally set as 15 minutes. Note that the targeter employed in FreeFlyer uses numerical partial derivatives of only the left hand side of Equation 5, resulting in an attenuated free-variable update at each iteration. Employing a more traditional approach that considers the partial derivatives of the free-variables within the entire expression may require adjustments to tolerances or weighting factors. Maneuvers are executed if they exceed the threshold of 3 cm/s in magnitude. Davis et al. explores the Gateway spacecraft orbit maintenance algorithm in detail.[3]

GEOMETRIC CONSIDERATIONS FOR ECLIPSE AVOIDANCE

An eclipse occurs when a spacecraft traverses through the shadow of a nearby astronomical body. In the lunar vicinity, both Earth and Moon eclipses may impact mission operations. Power and thermal mission constraints limit the allowable time in an eclipse to less than 90 minutes for the Gateway and Orion crew vehicle. Observing the 9:2 NRHO in simplified Sun-Moon and Sun-Earth rotating frames allows for the smaller body's shadow to be visualized relative to the orbit since the shadow is fixed along the positive x-axis in the respective Sun-Moon or Sun-Earth rotating frame. Figure 1 illustrates the CR3BP 9:2 NRHO in the Earth-Moon, Sun-Moon, and Sun-Earth rotating frames.* The bodies are assumed to be coplanar for ease of visualization, here. Note, to plot an Earth-Moon CR3BP orbit in a Sun-secondary rotating frame, an epoch

*As computed in the CR3BP, orbital properties of the L2 9:2 lunar synodic resonant NRHO are: perilune altitude of approximately 1450 km, apolune altitude of approximately 69500 km, and orbital period of approximately 6.56 days.[8]

must be selected for the spacecraft. Selection of epoch drives the phase of the spacecraft in the orbit relative to the shadow of the occluding body and thus directly relates to eclipse avoidance properties.

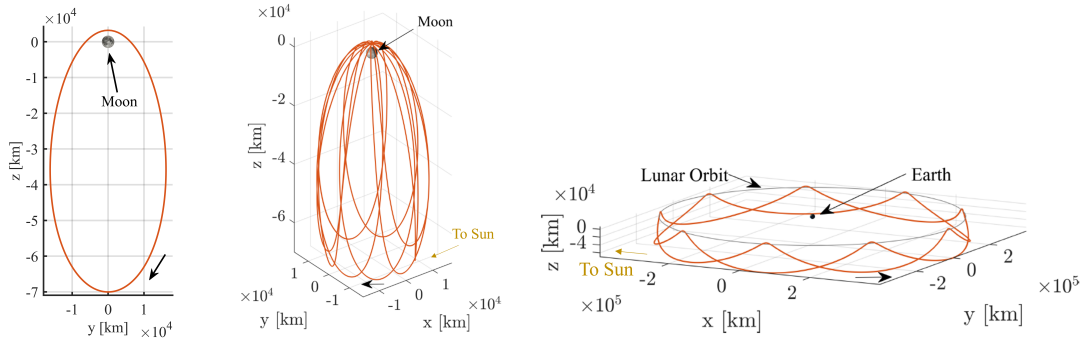

(a) Earth-Moon Rotating Frame (b) Sun-Moon Rotating Frame (c) Sun-Earth Rotating Frame

Figure 1. Earth-Moon L2 southern 9:2 lunar synodic resonant NRHO computed in the CR3BP

Geometrically, passages through lunar shadow are always nearby perilune, as is observed in Figure 1(b). Due to the high orbital velocity near perilune along the NRHO, lunar eclipse conditions are observed to always be less than 90 minutes, thus meeting the eclipse constraint. Conversely, spacecraft passages through Earth's shadow are typically longer in duration due to slower orbital velocity away from perilune, where passages through Earth's shadow usually occur along the NRHO (see Figure 1(c)), and the larger size of the Earth's shadow compared to the Moon's shadow as observed at the NRHO's distance from Earth. Passages through Earth's shadow can extend longer than the 90 minute constraint without mindful trajectory design.

Insight gained from the motion of the Moon through the Sun-Earth system enables a geometry-based eclipse avoidance strategy. This investigation focuses on avoiding Earth eclipses. The linear alignment of the Sun, Earth, and Moon indicates a spacecraft is at risk of passing through the shadow of the Earth. The Moon, and thus a spacecraft nearby the Moon in an NRHO, is closest in proximity to the Earth's shadow when it is in opposition with the Sun, i.e., during a "full Moon." Since in reality, the orbital plane of the Earth-Moon system is not coplanar with the ecliptic plane, the Moon does not pass through the Earth's shadow each month (such a passage results in a lunar eclipse as observed from Earth). A more realistic Sun-Earth rotating coordinate frame where the Moon is not coplanar is leveraged to accurately visualize the eclipse scenario. This Sun-Earth rotating frame is represented in Figure 2. The Sun-Earth rotating frame is defined with underlined quantities, where the $\underline{x}$-axis points from the Sun to the Earth, the $\underline{z}$-axis points along the angular momentum vector of the Sun-Earth orbital plane (ecliptic plane), and the $\underline{y}$-axis completes the right-handed, orthonormal triad. The origin of the coordinate frame is placed at the barycenter of the Sun-Earth system ($\underline{B}$).

The ecliptic angle is defined to characterize the location of the Moon relative to the Earth's shadow, which lies along the $\underline{x}$-axis. Consider a one-sided map recording the passes of the Moon through the $\underline{xz}$-plane in Figure 2. The one-sided definition records instances when the Moon passes from strictly negative to positive values of $\underline{y}$, i.e., the right side of the $\underline{x}$-axis from the Earth. The ecliptic angle (α) is illustrated in Figure 3. The vector $\mathbf{r}_{EM} = [x_{EM}\ y_{EM}\ z_{EM}]^T$ is directed from the Earth to the Moon in the Sun-Earth rotating frame, and the angle is computed by

$$\alpha = tan^{-1}\left(\frac{z_{EM}}{x_{EM}}\right) \tag{6}$$

The ecliptic angle is measured at each full Moon to determine the Moon's proximity to the Earth's shadow. The ecliptic angle evolves across each year due to the annual precession of the Moon's orbit in the Sun-Earth rotating frame. The progression of ecliptic angle is represented in Figure 4. The epoch starts at the full Moon that occurs on December 27th, 2023. Each blue dot along the curve represents the ecliptic angle at

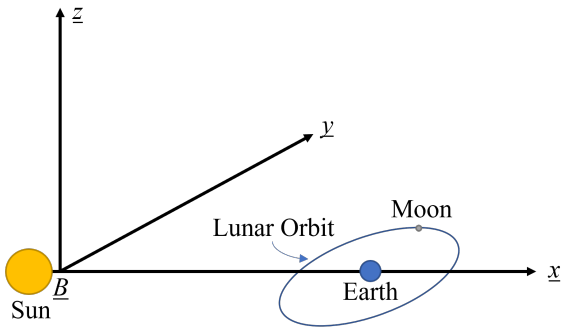

Figure 2. Sun-Earth rotating frame with non-coplanar Moon orbit; not to scale

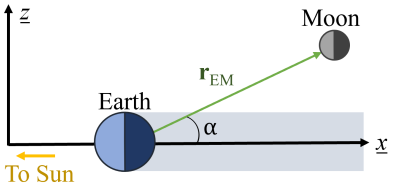

Figure 3. Ecliptic angle of the Moon relative to the *x*-axis of the Sun-Earth rotating frame; not to scale

the successive full Moon, e.g., the first dot at index zero is the December full Moon, while the dot at index four corresponds to the fourth full Moon of 2024, that is, in April. There exists a trend in the frequency and amplitude of the sinusoidal motion. The Moon's orbital plane about the Earth is inclined approximately 5.15° from the ecliptic plane. Thus, the inclination of the Moon's orbit bounds the upper and lower limits of the ecliptic angle. At the lunar distance, the Earth's shadow encompasses the ecliptic angles within approximately -1.25 to 1.25 degrees. When the ecliptic angle of the Moon is within the range, the Moon passes through the shadow of the Earth. As illustrated in Figure 4, the third and ninth full moons of 2024, in March and September, respectively, occur within the ecliptic angle range that corresponds to lunar eclipse. The same methodology can be used to determine the ecliptic angle for other months and years.

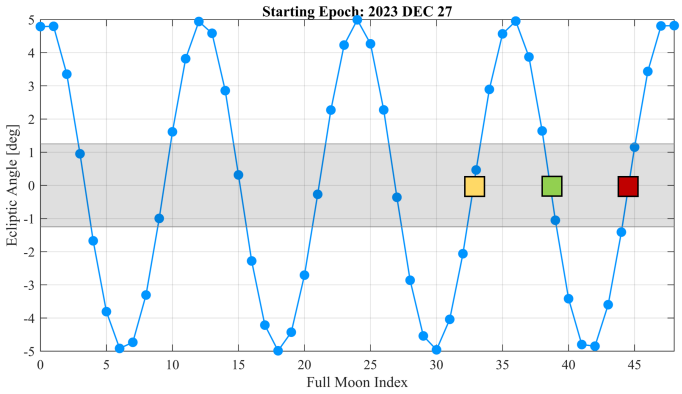

Figure 4. Ecliptic angle of the Moon relative to the *x*-axis of the Sun-Earth rotating frame for December 2023 through December 2024

Since the Earth-Moon system is inclined relative to the ecliptic plane, the same portion of the 9:2 NRHO does not pass through the Earth's shadow during each subsequent full Moon. That is to say, if a particular region of the NRHO is within the Earth's shadow during one full Moon, it may not be shadowed at the next full Moon. The ecliptic angle directly drives which portion of the NRHO may be subjected to passage through Earth's shadow in the time frame near a full Moon, simply based on geometry. This concept is illustrated in Figure 5. Note, the red bands along the NRHO indicate the portion of the NRHO that passes through the Earth's shadow. Although at the instant of the image, i.e., precisely at the full Moon, the orbit appears to pass *around* the Earth's shadow for α-angles greater than 1.25°, recall that the shadow of the Earth is not stationary in the Earth-Moon rotating frame, and is 'sweeping' across the image from right to left and thus passing over the NRHO portions in red. Additionally, note that for each red band along the NRHO, there is an additional red region that is offset from it by 4.5 revolutions. This second region exists due to the fact that the Gateway NRHO is resonant with two synodic periods of the Moon (i.e., a 9:2 synodic resonance); thus, if a spacecraft is at a particular TA, γ, and is within the Earth's shadow one month, the following full Moon will see the spacecraft at a TA associated with propagating 4.5 revolutions downstream. This downstream TA is not equivalent to γ. As an example, passages through TAs 190° and 163° occur approximately 4.5 revolutions apart in the 9:2 NRHO. In the higher fidelity ephemeris model, this offset may not be precisely equivalent to 4.5 revolutions since the period of the NRHO varies from revolution to revolution.[9] A spacecraft in either red region is at risk for passage through Earth's shadow.

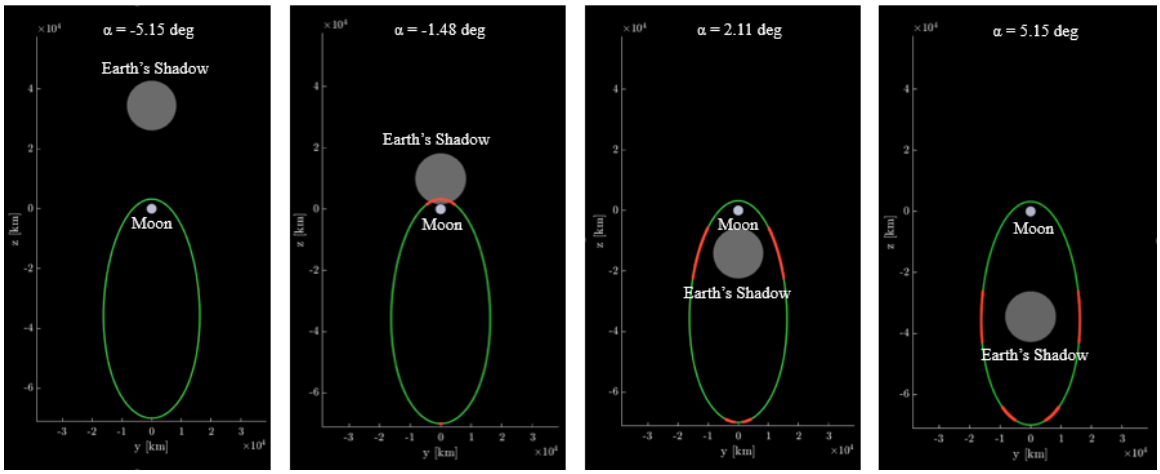

Figure 5. Portion of the 9:2 NRHO within the shadow of the Earth for various ecliptic angle values

Over the course of a full year or longer, only spacecraft in the phases dictated by TA values between approximately 163°-170° and 190°-197° at a full Moon are predicted to remain outside the Earth's shadow. As a result, for the fifteen-year lifespan of Gateway, there are two general phases that are Earth eclipse avoidant. The phase of the 2017 Gateway baseline NRHO is such that on December 27, 2023 (the full Moon epoch), the Gateway is at approximately 191° in TA.[4] An alternative eclipse-avoidant phase exists for a spacecraft within the first band of TA, that is, between 163°-170° TA on December 27, 2023. A spacecraft in the nominal phase (i.e., the phase selected the Gateway program[4]) passes through perilune concurrently with a spacecraft in the alternate phase passing through apolune.

For shorter time spans, spacecraft in other phases can remain outside the Earth's shadow. As an example, a spacecraft can be in any phase along the NRHO and remain outside the Earth's shadow over the four month span starting on April 23, 2024, during which the ecliptic angle is always less than -1.25° at the full Moon, as is depicted in Figure 4. As a point of reference, the 2017 baseline is at TA = 199° on April 23, 2024. Two different phases of the NRHO computed in the point mass ephemeris model between April 23, 2024 and August 19, 2024 are illustrated in Figure 6 in the Sun-Earth rotating frame. The green curve has an initial TA of 180° and the red curve has an initial TA of 199°. Stars mark the location of the spacecraft on 23 April

2024. Alternatively, for a four month propagation with a start epoch of 19 August 2024, the ecliptic angle

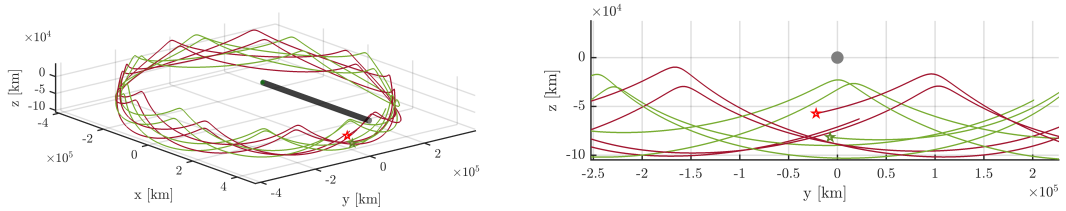

(a) Sun-Earth rotating frame

(b) View along the Earth's shadow

Figure 6. Two phases within the 9:2 NRHO in the point-mass ephemeris model with start epoch April 23, 2024

of the Moon grows greater than -1.25°. Selecting NRHO phases outside of the Earth eclipse-avoidant zone (approximately 163°-170° and 190°-197° TA at the full Moon epoch) results in passages through or near eclipse conditions on the spacecraft. The same spacecraft phases selected for Figure 6 are again propagated and plotted in Figure 7. Note that the spacecraft in the TA = 180° phase, plotted in green, passes very nearby the Earth's shadow, denoted in grey and projecting out of the page. The ecliptic angle over the time frame considered and phase of the spacecraft within the NRHO directly determine if a spacecraft is at risk of Earth eclipse conditions.

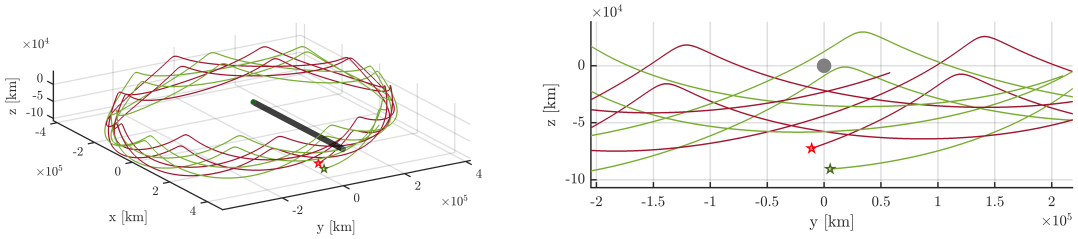

(a) Sun-Earth rotating frame

(b) View along the Earth's shadow

Figure 7. Two phases within the 9:2 NRHO in the point-mass ephemeris model with start epoch August 19, 2024

REFERENCE GENERATION

Due to the sensitive dynamics of the NRHO, creating a many-revolution ballistic trajectory in an ephemeris model that remains geometrically similar to the CR3BP NRHO presents a unique set of challenges. Even with an appropriate initial condition selection, purely propagating in a higher-fidelity ephemeris model (and even in the CR3BP) cannot generate a many-revolution baseline. Differential corrections or other numerical techniques are necessary to generate long-duration NRHOs that remain in quasi-periodic bounded motion similar to the CR3BP geometry.

Maintaining a particular phase of the NRHO precisely enough such that eclipses from the Earth are avoided presents additional restrictions and difficulty, especially in the case of a 9:2 NRHO. The shadow of the Earth must pass through a relatively narrow gap between perilune peaks of the NRHO, as plotted in the Sun-Earth rotating frame.[10] This fact is depicted in Figure 1(c). Due to this narrow gap, there is a relatively small margin in allowable TA at each successive full Moon for a spacecraft moving along the NRHO to maintain Earth-eclipse avoidant properties. The baseline generating approach must include this consideration to satisfy mission constraints on allowable eclipse passage durations.

Original Baseline Generation Strategy

The Gateway baseline generated by Lee in 2017, the "2017 baseline," introduced the first many-revolution eclipse-avoidant 9:2 NRHO baseline generated via careful phasing of a synodic resonant NRHO. The 2017 baseline includes perturbations from the *N*-body ephemeris model, particularly, the Earth, Moon, Sun, and Jupiter barycenter.[2,4] The Moon is modeled using 8x8 spherical harmonics and all other bodies are considered as point masses. To ensure the baseline is applicable and unbiased regardless of spacecraft properties, no solar radiation pressure, drag, spacecraft noise, navigational errors, or insertion errors are included. An iterative process is used to develop the 15-year pseudo-ballistic trajectory and is described in detail by Lee.[2] In summary, a forward/backward multiple-shooting differential correction scheme is used to generate a 27-revolution seed trajectory (approximately 6 months in duration) using an initial guess from the CR3BP.[10] Then, to extend the duration of the ephemeris trajectory, a receding-horizon targeting approach is utilized.[10] In the case of the NRHO baseline, an initial state near perilune from the converged or nearly converged multiple-shooter solution is used to initialize the process. A small velocity perturbation is solved for near apolune 0.5 revolutions later such that the Earth-Moon rotating x-velocity is equal to zero at the xz-plane crossing near perilune 11 revolutions downstream. This downstream targeting scheme is continued to generate multi-year long solutions that avoid Earth-eclipse conditions. The process is terminated if eclipse avoidance becomes difficult to achieve. The total process (multiple-shooter seeding a receding-horizon approach) is repeated with various initial conditions until a 15-year Earth-eclipse avoidant baseline is obtained. On average, the velocity adjustments in the receding-horizon solution are of magnitude 1.86 mm/s per NRHO revolution.

The geometry of the 2017 baseline orbit remains similar to the CR3BP NRHO over the 15-year duration. The baseline is illustrated in Figure 8 in the Sun-Earth rotating frame; the shadow of the Earth is projected out of the page. Note that the familiar 9 peak and 9 trough "crown-like" geometry, obvious in Figure 1(c), is apparent, however, the geometry is 'smeared' due to perturbations in the higher-fidelity ephemeris model. The

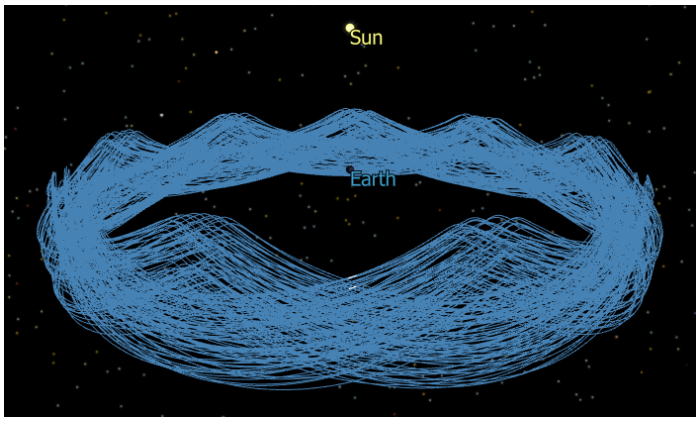

Figure 8. 2017 baseline in Sun-Earth rotating frame; white segments indicate Earth eclipses

perilune altitude, apolune altitude, and orbital period measured between perilune passages vary along each revolution of the baseline. Table 1 contains information on the minimum, maximum, mean, and standard deviation for these parameters for the 2017 baseline. The mean apolune altitude and mean orbital period are nearly equal to those predicted by the CR3BP 9:2 NRHO counterpart. However, the CR3BP perilune altitude is smaller than the mean baseline perilune altitude, in fact, the minimum baseline perilune altitude is nearer to the value predicted by the CR3BP. One goal of Gateway orbit maintenance is to ensure perilune remains above 1400 km in altitude, thus, it is critical that the baseline trajectory, which provides the target for OM, remains outside this minimum perilune constraint with some amount of buffer. Figure 9 illustrates the variation in perilune altitude over the revolutions of the baseline NRHO. The lowest perilune passages occur between 2031 and 2033. The minimum perilune passage is 1458.2 km along the baseline plotted in Figure 8, thus the constraint is satisfied.

Table 1. Orbital characteristics for the 2017 baseline

	Min	Mean	Max	StDev
Apolune Altitude (km)	68267.1	69363.0	70112.0	506.7
Perilune Altitude (km)	1458.2	1629.1	1819.6	66.5
Period (days)	6.26	6.56	6.76	0.14

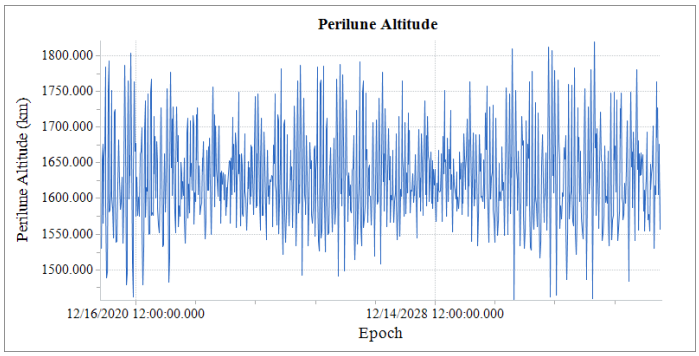

Figure 9. Perilune altitude along the 2017 baseline depicted in Figure 8

Eclipse duration limits due to thermal and power limitations drive a challenging 90 minute maximum eclipse passage time constraint for the Gateway spacecraft. In this analysis, any passage through the Earth's penumbral or umbral shadow is considered as an eclipse. The duration of passages through shadow are delineated in Table 2. Two Earth eclipses longer than 90 minutes in duration exist along the this baseline–one on 12 July 2033 and one on 01 July 2034. Both of these passages through the Earth's penumbral shadow are on the order of approximately 2 hours in duration. It is expected that a new baseline would be generated before the spacecraft would pass through these shadows, thus their existence in the baseline is of minimal concern.[2] In Figure 8, the passages through the shadow of the Earth are highlighted in white.

Table 2. Passages through Earth's shadow along the 15-year 2017 baseline

Earth Shadow Event	Date/Time	Duration (mins)
Entry into Penumbral Shadow	Jul 12 2033 13:53:33	-
Exit from Penumbral Shadow	Jul 12 2033 16:02:00	128.4
Entry into Penumbral Shadow	Jul 01 2034 22:42:47	-
Exit from Penumbral Shadow	Jul 02 2034 00:42:04	119.3

Automated Multi-Tier Multiple-Shooter Baseline Generation Strategy

As an alternative to the intensive hands-on approach to generate a singular reference trajectory, the original baseline generation method, an automated multi-tier multiple-shooter baseline generation strategy is developed. In this strategy, revolutions from a CR3BP NRHO are stacked and patchpoints from these revolutions seed an initial guess in a forward-shooting fixed-time multiple-shooter differential corrections scheme in the higher-fidelity point mass Earth-Moon-Sun ephemeris model. Due to the sensitivity of the NRHO and numerical challenges associated with inverting large matrices accurately, progressively longer duration segments are corrected and 'stitched' together. The basics of the multiple-shooter differential corrections scheme are described in detail by Zimovan Spreen in a 2021 Ph.D. dissertation.[8] If the algorithm does not follow a multi-tier approach, challenges in maintaining the geometry of the NRHO in the Sun-Earth rotating frame arise. To transition CR3BP patchpoints from a time-invariant system into a non-autonomous higher-fidelity ephemeris model, a selection of initial epoch must be made. Within this algorithm, the initial condition for the ephemeris solution is based on a specified true anomaly along the NRHO at a given full Moon on a spec-

ified month, e.g., a true anomaly of 194° along the NRHO for the full Moon in December 2025 (occurs on 4 December 2025). This true anomaly/date combination corresponds to the phase of the Gateway NRHO. Together, a true anomaly and epoch date fully defines the phasing of the resulting higher-fidelity baseline orbit, and the method is such that the phasing is maintained over the course of the generated baseline. No additional mathematical constraints are required to maintain the geometry of the higher-fidelity solution. With appropriate phase selection of the initial guess, an eclipse-avoidant baseline is produced.

The initial portion of the algorithm is developed in Matlab. In this portion, the CR3BP patchpoints are transitioned to an Earth, Moon, and Sun point-mass ephemeris model. No solar radiation pressure, drag, spacecraft noise, navigational errors, or insertion errors are included to ensure the baseline is applicable and unbiased regardless of spacecraft properties. Relative and absolute tolerances are set to 1e-12. Initially, segments with a duration of 2 synodic months (equivalent to 9 revolutions on the 9:2 NRHO) are converged using 3 patchpoints per revolution equally spaced in time with one patchpoint per revolution at apolune in the initial guess. The initial state along each segment is fixed in time such that each two-month segment is continuous in time with the next. The two-month long segments are converged to a 2-norm tolerance of 1e-10. The tolerance is a non-dimensional value and corresponds to 38 mm in position components and 0.0001 mm/s in velocity components. An attenuation factor is enforced such that the 2-norm of the update vector is less than 0.1. The attenuation factor aids in convergence to a geometry that remains similar to the CR3BP initial guess. Once all 2-month duration segments are converged, the patchpoints from the resulting solutions are stacked into 2-year long segments. At this time, 3 patchpoints per revolution are maintained in the algorithm. For the 2-year long segments, convergence is reached when the infinity-norm of the constraint vector is less than 1e-9. A non-dimensional tolerance of 1e-9 corresponds to 38 cm in position components and 0.001 mm/s in velocity components. Typically, a 2-norm on the order of 1e-10 and an infinity-norm on the order of 1e-11 or 1e-12 is reached at convergence. Again, an attenuation factor is included such that the update to the free-variable vector has a 2-norm of less than 0.1. Three 2-year long segments are then stitched together in order to converge 6-year long segments. These segments again contain 3 patchpoints per revolution along the NRHO and are converged to an infinity-norm of 1e-9. Similar to the previous tier, a 2-norm on the order of 1e-10 and an infinity-norm on the order of 1e-11 or 1e-12 is typically reached at convergence. Again, an attenuation factor is implemented to limit the maximum size of the update to the free-variable vector to 0.1. Finally, all 6-year segments are combined to form the full many-year baseline trajectory. Three patchpoints per revolution are maintained, however, the maximum update of the free variable vector is now constrained to be less than or equal to 0.05. The tolerance at this tier of the algorithm is set as 1e-9. Convergence is reached in approximately 10 iterations at this level. Fewer than 10 iterations are typically seen at each earlier tier to reach convergence for each segment. Using this strategy, baselines of 30+ years are demonstrated as able to be generated, however, 15-20 years is recommended in order to maintain a tight perilune radius spread in the final solution. To converge a 20 year baseline, the Matlab portion of the algorithm requires approximately 90 minutes of wall time. Shorter baselines require significantly less time to compute as the time required for inversion of matrices scales exponentially with the size of the matrix. As a sample, a 24 month baseline can be computed in under 3 minutes. Integration is performed in Matlab using an integrator in C++ from the GNU Scientific Library (GSL).[11]

After convergence in Matlab, the patchpoints are imported into FreeFlyer, a commerical off the shelf astrodynamics software package.[7] The number of patchpoints is reduced to one per revolution, with each patchpoint at apolune. Then, a multiple-shooting algorithm is used to enforce continuity in position and velocity in an ephemeris model that incorporates spherical harmonics of the Moon. If desired, additional perturbing bodies or other perturbing forces can be incorporated into the baseline at this time. Spherical harmonics of degree and order 8 as well as degree and order 16 have been successfully incorporated in the model used to the generate a baseline NRHO, as has solar radiation pressure. Trajectory segments are propagated with a Runge-Kutta 8(9) integrator with a tolerance of 1e-12. The tolerance on continuity is enforced to a level of 1e-10 on the 2-norm of the continuity constraint vector. The tolerance of 1e-10 is a non-dimensional value and corresponds to 38 mm in position components and 0.0001 mm/s in velocity components. The multi-tier strategy is summarized in Figure 10.

It is important to note on the numerical challenges associated with computing a long-duration baseline.

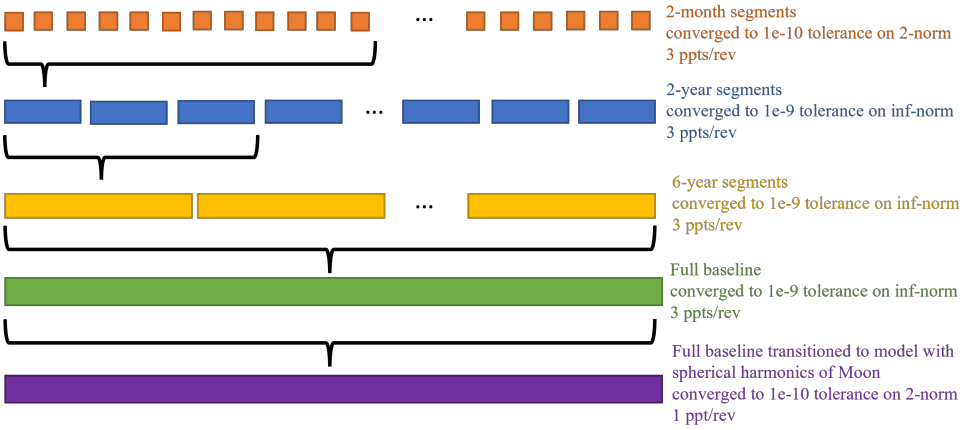

Figure 10. Multi-tier multiple-shooting baseline generation algorithm schematic

Table 3. Accuracy and computational time comparison of various inverse methods in Matlab for a Jacobian matrix of size 19596 by 19602

Update Equation	Identity Computation	Time	Accuracy
`DF'*(inv(DF*DF')*F)`	`inv(DF*DF')*DF*DF'`	191.0 sec	O(1e-9)
`DF'*((DF*DF')\F)`	`(DF*DF')\DF*DF'`	62.2 sec	O(1e-12)
`DFs'*(inv(DFs*DFs')*F)`	`inv(DFs*DFs')*DFs*DFs'`	5.4 sec	O(1e-5)
`DFs'*((DFs*DFs')\F)`	`(DFs*DFs')\DFs*DFs'`	0.02 sec	O(1e-8)

Patchpoints can be 'deleted' from the baseline to reduce the size of the free-variable and constraint Jacobian matrix to reduce the duration of time required to perform an inverse and to increase the accuracy of that inverse. However, even if patchpoints are omitted, it is important to note that the convergence tolerance of the multiple-shooting algorithm is limited by the accuracy of the inverse of the Jacobian matrix. It was observed that maintaining the Jacobian matrix as a fully-populated matrix (i.e., not defining the matrix using Matlab's `sparse` command) increases the accuracy of the inverse computation. The inverse should be taken as `DX = DF'*((DF*DF')\F);` where `DX` is the update to the free variable vector, `DF` is the Jacobian matrix, `F` is the constraint vector containing continuity constraints. The apostrophe operator yields the complex conjugate transpose of a matrix in Matlab and the backslash operator yields the inverse of the preceding matrix. This operator computes the inverse using Gaussian elimination and uses less computational time and produces a more accurate result than the Matlab `inv()` command.[12] Table 3 displays four different strategies that can be used to compute the update to the free variable vector for a large, sparse matrix. These expressions are in column 1. In this table, `DFs` is equivalent to `sparse(DF)`. Column 3 shows the wall time necessary to compute the identity matrix defined in column 2, and the accuracy of the identity matrix (i.e., measured as how close the zero values are to zero) is displayed in column 4. The selected algorithm, highlighted in yellow is is slower than two of the other options, however is significantly more accurate than the other three strategies. Matlab is used for the computation of the free-variable updates in all phases of the process; Matlab is called externally by FreeFlyer to preserve the high level of accuracy of this computation in both portions of the algorithm.

Figure 11 illustrates a 20-year ballistic L2 southern 9:2 lunar synodic resonant NRHO baseline generated using the automated multi-tier approach. The NRHO in this figure is plotted in the Sun-Earth rotating frame and the shadow of the Earth is projected out of the page. This baseline includes 8x8 spherical harmonics for the Moon and possesses a start epoch on 04 DEC 2025. The initial TA at the full Moon of the start epoch is 193°. This baseline is in the nominal Gateway phase originally defined in the 2017 baseline. Orbital characteristics for this updated 20-year baseline are displayed in Table 4. The minimum and maximum

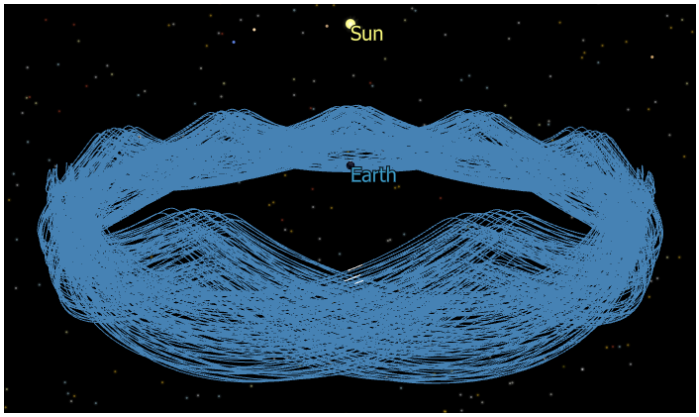

Figure 11. 20-year 9:2 NRHO baseline in Sun-Earth rotating frame generated with multi-tier multiple-shooter strategy; white segments indicate Earth eclipses

apolune altitudes are spread slightly larger than the minimum and maximum apolune altitude of the 2017 baseline, as compared to Table 1. However, the mean apolune altitude is within 6 km of the mean from the 2017 baseline. The standard deviation for the apolune altitude of the new baseline is smaller than the 2017 baseline's by 2 km, indicating that overall, the apolune altitude is more consistent from revolution to revolution in the newly generated baseline. Similarly, the spread of perilune altitude is slightly larger in the new baseline, however, the mean perilune altitude is nearly identical between the two baseline trajectories. Finally, the period of each revolution, as measured from perilune to perilune state along the NRHO is nearly identical between the two baselines. Note that the minimum perilune passage is 1440.7 km, thus, the 1400 km minimum perilune altitude constraint is satisfied. The perilune passage altitude for each revolution is

Table 4. Orbital characteristics for the 20-year baseline from Figure 11

	Min	Mean	Max	StDev
Apolune Height (km)	68196.4	69366.7	70129.6	504.7
Perilune Height (km)	1440.7	1629.8	1829.3	66.63
Period (days)	6.25	6.56	6.76	0.14

plotted in Figure 12. Similar to the 2017 baseline, the minimum perilune altitude passages occur between 2032 and 2033 indicating that, perhaps, geometry of perturbing bodies at this epoch drives lower perilune passage altitudes.

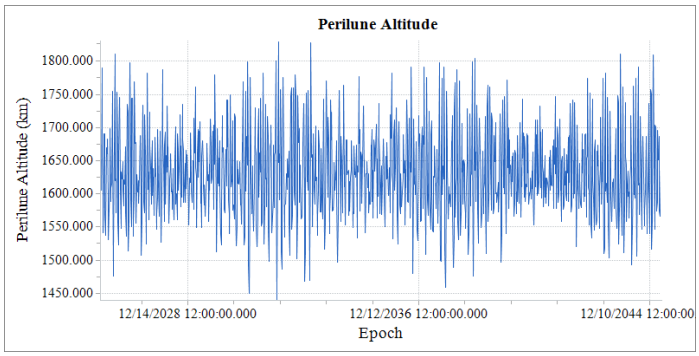

Figure 12. Perilune Altitude along the 20-year 9:2 NRHO baseline in Figure 11

Table 5 lists the passages through the Earth's shadow along the updated 20-year baseline. There are five

transits through the Earth's shadow, including one umbral shadow passage. Similar to the 2017 baseline, only two of the eclipse passages violate the 90-minute eclipse duration constraint. Note that the eclipses on 12 July 2033 and 02 July 2034 occur in both the 2017 baseline and the updated baseline. The duration of these two eclipses are reduced to under 90 minutes in the updated baseline. The two eclipses in the updated baseline that are longer than 90 minutes occur in 2039 and 2040, beyond the span of the 2017 baseline.

Table 5. Passages through Earth's shadow along the 20-year baseline generated using the automated multi-tier multiple-shooting approach

Earth Shadow Event	Date/Time	Duration (mins)
Entry into Penumbral Shadow	Sep 11 2030 15:21:09	-
Exit from Penumbral Shadow	Sep 11 2030 16:15:03	53.9
Entry into Penumbral Shadow	Jul 12 2033 14:34:57	-
Exit from Penumbral Shadow	Jul 12 2033 15:25:16	50.3
Entry into Penumbral Shadow	Jul 01 2034 23:06:14	-
Exit from Penumbral Shadow	Jul 02 2034 00:20:13	74.0
Entry into Penumbral Shadow	Mar 10 2039 20:00:41	-
Exit from Penumbral Shadow	Mar 10 2039 23:24:09	203.5
Entry into Penumbral Shadow	Feb 28 2040 04:26:26	-
Entry into Umbral Shadow	Feb 28 2040 05:58:53	-
Exit from Umbral Shadow	Feb 28 2040 06:59:19	60.4
Exit from Penumbral Shadow	Feb 28 2040 08:29:55	243.5

Although the sample case illustrated here is a 9:2 lunar synodic resonant NRHO in the nominal Gateway phase, the process is not limited to this particular NRHO or to the eclipse-avoidant nominal phase of the Gateway. As a sample, Figure 13 shows six alternatively phased 9:2 NRHOs computed using the multi-tier algorithm at shifted phases relative to the nominal baseline. The start epoch for each NRHO is 14 March 2025 and each orbit is 24 months in duration. The blue dot in each image illustrates the same perilune pass in each NRHO; this marker aids in visualizing the different phases across each solution. The Earth's shadow is shown projecting out of the page; alternatively phased NRHOs are not oriented to geometrically avoid eclipses.

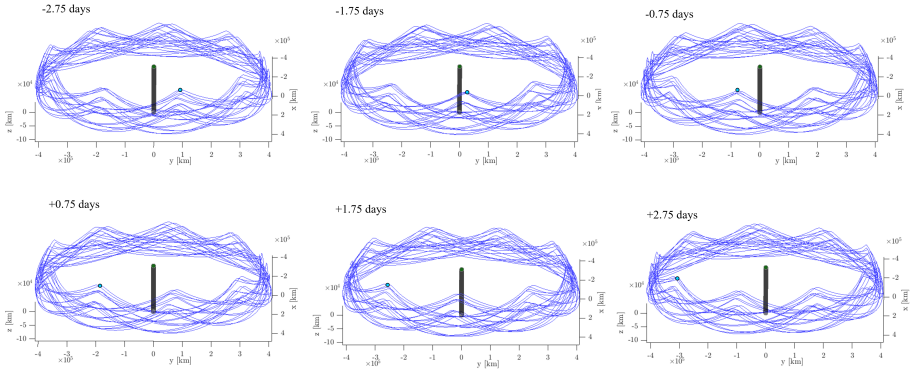

Figure 13. Alternatively phased 9:2 NRHOs in the Sun-Moon rotating frame

Comparison of Orbit Maintenance Cost

The baseline trajectory is used to produce the targets for the Gateway OM algorithm. Other analyses for the spacecraft (e.g., propellant budget and trajectory planing for visiting vehicles) is reliant on states obtained

from the baseline trajectory, as well. To compare the new baseline, generated using the multi-tier approach, to the baseline NRHO that is currently in use for Gateway analyses, that is, the 2017 baseline, a comparison of orbit maintenance costs over an identical time span is performed. Figures 14 and 15 serve as a comparison of the stationkeeping performance for a spacecraft maintained relative to each baseline. The start epoch in each case is 05 December 2025, and stationkeeping is performed for 5 years. One hundred Monte Carlo trials are executed. Perturbations on the spacecraft are described in the Background section of this paper, specifically, the subsection entitled 'The N-Body Ephemeris Model.' Figures 14(a) and 15(a) illustrate the burn magnitude for each OMM along the 5-year span. Burns that only target the rotating x-velocity are of lower magnitude than maneuvers that target both the rotating x-velocity and the perilune passage time or phase constraint. In both cases, approximately 32% of OMM burn opportunities are executed over the five year span with a mean magnitude of 5.4 cm/s for each maneuver. Figures 14(b) and 15(b) display the cumulative OM cost. The 2017 baseline yields a total OM cost with a mean value of 4.84 m/s over five years, or annually, an average cost of 0.96 m/s per year. The newly generated baseline results in a five-year OM cost of 4.94 m/s over five years, or 0.98 m/s per year. The variations in the mean cost are likely a result of the limited Monte Carlo analysis; additional trials would increase the resolution of the results. The perilune passage time errors, or the difference in perilune passage time of the spacecraft versus the baseline over each revolution is plotted in Figure 14(c) and Figure 15(c). In each case, the perilune passage time is observed to be bounded between ± 0.8 hours of the reference perilune passage time. Finally, in Figures 14(d) and 15(d), the position error at the perilune passage time as measured in the J2000 inertial frame is recorded. The error is measured as the difference between the perilune state along the trajectory flown by the Monte Carlo trial spacecraft and the corresponding perilune state of the baseline NRHO. For both baselines, the position errors are similar in magnitude and in behavior. The growth in position errors as the number of revolutions along the baseline increases, previous work by Davis et al. shows that adding a damping maneuver can reduce these errors.[3]

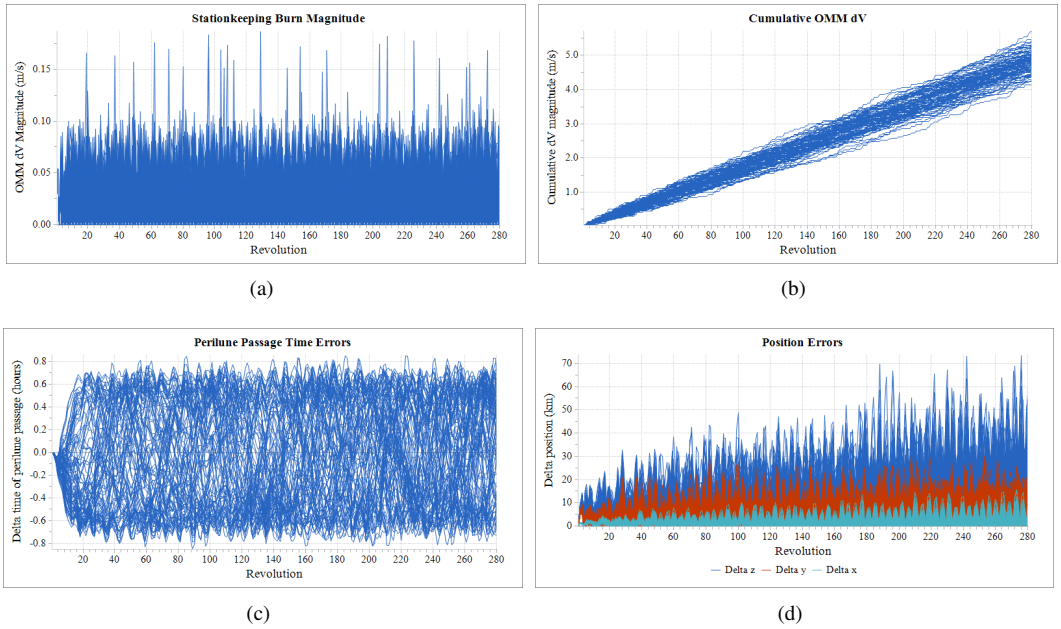

Figure 14. Orbit maintenance performance for the 15-year baseline generated in 2017

ORBIT MAINTENANCE PHASE CHANGE STRATEGY

To enable or facilitate various mission opportunities, it may be desirable to move the Gateway from the nominal phase into a shifted phase. Modified perilune passage time targets in the OM algorithm can be used to change phases of the NRHO over the course of multiple revolutions. A preliminary investigation into the

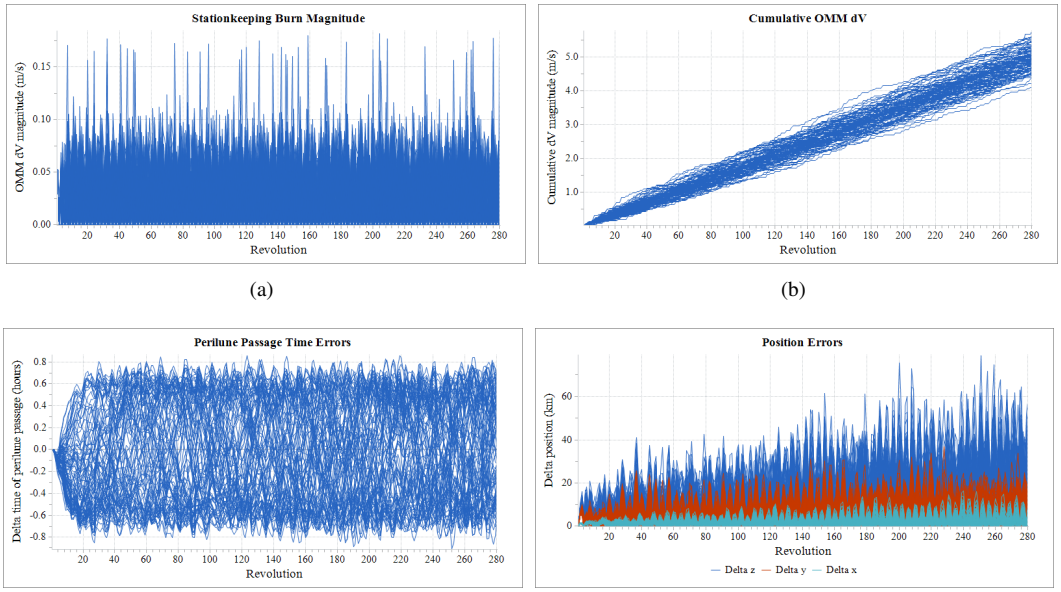

Figure 15. Orbit maintenance performance for the 20-year multi-tier generated baseline

OM phase change approach is offered by Davis et al.[5] As an alternative to Equation 4 in the OM algorithm, a weighted perilune passage time that has been modified from the nominal reference perilune passage time is used to shift the phase of the NRHO. Equation 4 is then replaced by

$$t_{targ} = W_t \left(t_{pref} + \Delta t - t_p \right) + t_p \tag{7}$$

where W_t is an empirically selected weighting factor, here 0.3, t_{pref} is the perilune passage time along a baseline NRHO, and t_p is the perilune passage time achieved by the maintained spacecraft after each iteration. In Equation 7, the value of Δt is a function of the number of revolutions, N, over which a long-lead phase shift is executed, and the magnitude of the total phase shift desired, t_{shift}. For each revolution, i, during the phase shift process, Δt is defined as

$$\Delta t = i \frac{t_{shift}}{N} \tag{8}$$

The shift rate is defined as t_{shift}/N. Once the new phase is reached, i.e., $\Delta t = t_{shift}$, the nominal OM approach is resumed at the new phase. In the nominal OM algorithm, t_{pref} and v_{xref} can be obtained from a phase-shifted baseline. The automated multi-tier multiple-shooting baseline generation approach is utilized to generate this alternatively-phased NRHO. If the new phase is only maintained for a few revolutions or if an alternatively-phased baseline NRHO is not available, OM can be performed using t_{pref} and v_{xref} from the nominal baseline, with t_{targ} defined as

$$t_{targ} = W_t \left(t_{pref} + t_{shift} - t_p \right) + t_p \tag{9}$$

It is recommended to return to the nominal OM approach using perilune passage time values obtained from a phase-shifted NRHO baseline within the equation for t_{targ}; OM costs return to the nominal level if a damping maneuver is added on the revolution corresponding to the switch in baselines from nominal to alternatively-phased or vice versa. Damping maneuvers add rotating y-position components into the targeting algorithm to effectively damp out oscillatory behavior when the spacecraft first reaches the new phase or returns from a phase change back to the nominal phase.[5] For short duration or small size phase changes, e.g., only remaining at a slightly shifted phase for a few revolutions, using Equation 9 as well as targeting v_{xref} from the nominal baseline is sufficient.

In a sample case, a phase change is used to successfully avoid the approximately 4-hour eclipse that occurs on 28 February 2040 in the multi-tier generated baseline depicted in Figure 11. A 2-year subsection of the baseline with a start epoch of 05 January 2039 is extracted for manipulation. The 2-year subsection of the reference is plotted in Figure 16 and the February 28 eclipse is marked with an arrow. This eclipse occurs along revolution 63 of this 2-year subsection of the baseline. To demonstrate the ability to avoid this eclipse

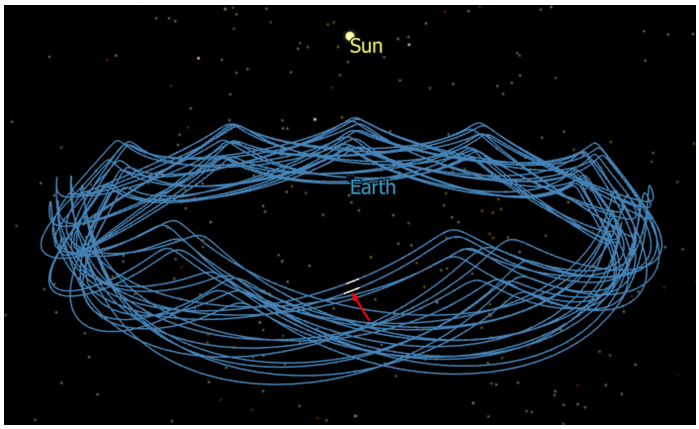

Figure 16. 2-year subsection of the mutli-tier baseline NRHO

in operations, a 10-hour phase change is used. The spacecraft is targeted to shift by 10 hours relative to the nominal baseline and then return back to the nominal phase. In this example, a shift of 10 hours denotes a case where the shifted spacecraft has a perilune passage time 10 hours later than the perilune passage time of a spacecraft in the nominal baseline. Over the first 51 revolutions, nominal OM takes place. At revolution 52, the phase shift begins. Over the next 5 revolutions, the shift in phase is targeted at a rate of 2 hours per revolution to target a total phase shift of 10 hours by revolution 56. In practice, there is a delay in achieving the full phase shift that lasts multiple revolutions. This delay is caused by the weighting factor on the periapse passage time targeting equation and the fact that at each OMM, downstream states at a perilune passage over 6 revolutions downstream are targeted. The 10-hour shifted phase is targeted to be held for the following 6 revolutions using the method denoted by Equation 9. After the sixth revolution, at revolution 62, the perilune passage time targeting equation is modified again to begin shifting the phase back to the nominal phase over the next 10 revolutions at a rate of 1 hour per revolution. Figure 17(a) shows the result of this targeting scheme as measured by perilune passage time of the spacecraft relative to the nominal baseline perilune passage time. In Figure 17(a), the maximum phase change is observed to occur at revolutions 63 and 64, that is, near the

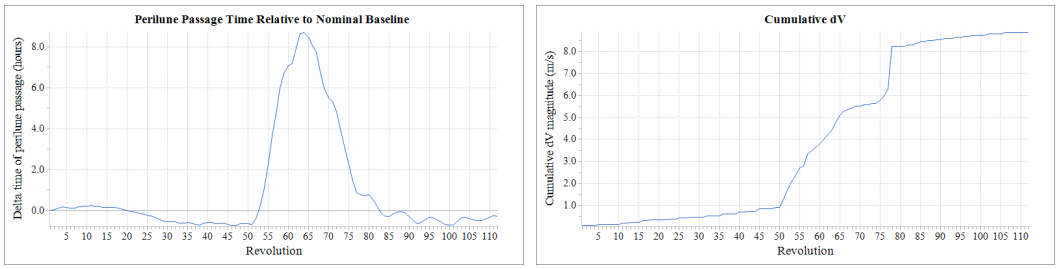

(a) (b)

Figure 17. 10-hour eclipse avoiding phase-change perilune passage time and cumulative maneuver cost

same revolution that the eclipse nominally occurs. The nominal phase is again achieved at approximately revolution 82 and perilune passage time of the spacecraft measured relative to the nominal baseline returns

to a similar pre-phase change magnitude. Figure 17(b) illustrates the cumulative maneuver cost for nominal OM and the eclipse-avoiding phase change. The phase change and return to the nominal phase requires approximately 7.2 m/s total. Further tuning on the rate of the phase change, i.e., the number of revolutions used to shift to the new phase and back, and size of the required phase change could be reasonably expected to reduce this overall cost. Figure 18 illustrates the resulting trajectory. Note that the eclipse marked with a red arrow in Figure 16 is no longer apparent as this passage through the Earth's shadow has been successfully avoided.

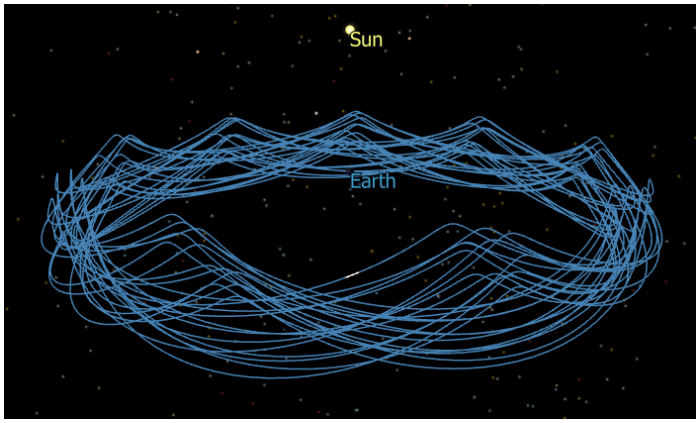

Figure 18. 2-year subsection of the mutli-tier baseline NRHO

There are two eclipse-avoidant phases of the NRHO, that is, the nominal Gateway phase and an alternative phase that passes perilune half a revolution ahead of (or equivalently, behind) a spacecraft in the nominal Gateway phase. Beyond applications for Gateway itself, this alternative phase offers an eclipse-avoidant parking orbit for a human lander, e.g., the reusable lander proposed by Blue Origin, among other applications.[13,14] In such applications, it may be necessary to transition from the nominal phase to the alternative phase or vice versa. To demonstrate this capability, a half-revolution phase change (approximately 3.28 days or 78.7 hours) is completed. To accomplish this large phase change using the OM phase change algorithm, many revolutions are needed due to a limited phase change rate per revolution.[5] Larger values of shift rate lead directly to large increases in overall cost to accomplish a phase change using this algorithm.[5] The phase change cost, in general, approaches a steady state when using a shift rate of approximately 1 hour per revolution, however, in this example, the duration that the spacecraft is out of an eclipse-avoidant phase may be prohibitive due to the possibility of eclipse. To determine the shift rate required, an additional constraint on the transition between phases can be enforced: the spacecraft should not pass through shadow during the transition revolutions. To meet this requirement, the majority of the phase change should occur in a favorable eclipse-avoidant geometry, regardless of the instantaneous phase of each transition revolution. An eclipse-avoidant geometry, regardless of phase in the NRHO, is available while the Moon is below the ecliptic, as is demonstrated by the example plotted in Figures 6 and 7. The Moon is below the ecliptic for six synodic months per year, thus the rate of phase change of the orbit, such that the majority of the phase change occurs when the Moon is below the ecliptic, should be approximately 3 hours per revolution (shifting 78.7 hours over 27 revolutions of the 9:2 NRHO in 6 synodic months). To accommodate the delay in the OM-based phase change algorithm, 25 transition revolutions, and thus 3.15 hours per revolution are selected for this example. Starting at an initial epoch of 05 December 2025, nominal OM is performed for one year and is continued till the Moon is "descending" through the ecliptic plane. OM is performed using Equation 4 using targets from the nominally phased eclipse-avoidant baseline presented in Figure 11. The Moon passes through the ecliptic plane two months later and the phase change is initiated. The green square in Figure 4 illustrates the Moon's approximate angle relative to the ecliptic plane at the start of the phase change. Note that the Moon is not at a full Moon condition at this epoch. The phase change is targeted to be completed at the epoch associated with the red square in Figure 4. Once at the new phase, targets are obtained from a reference possessing the

alternative eclipse-avoidant phase and OM is performed using Equation 4. The alternative eclipse-avoidant phase baseline was generated using the multi-tier multiple-shooting based phase change algorithm and also contains an 8 by 8 lunar gravity model.

In Figure 19(a), the trajectory history of a spacecraft performing this phase change is plotted. One year plus 9 revolutions in the nominal phase are plotted in blue, the phase-changing transition revolutions are plotted in green, and one year in the alternatively phased eclipse-avoidant baseline is plotted in pink. Note that the peaks associated with the green transition revolutions along the positive $\underline{x}$-axis (at the bottom of the image) are lower than the majority of peaks associated with the blue and pink portions of the trajectory in the same region. This occurrence is due to the fact that the transition revolutions are intentionally planned to occur while the Moon is below the ecliptic plane to avoid Earth shadows. Figure 19(b) illustrates the

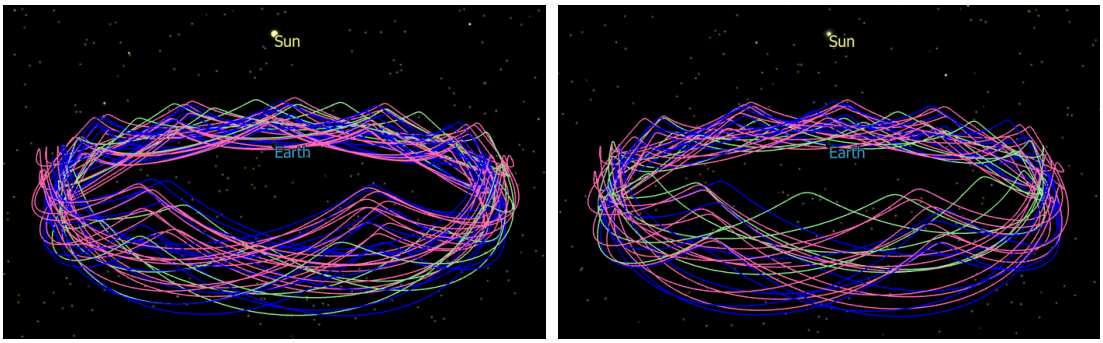

(a) Transition revolutions occur while Moon is below the ecliptic plane

(b) Transition revolutions occur while the Moon is above the ecliptic plane

Figure 19. Transition from the nominal Gateway phase to the alternative eclipse-avoidant phase

same phase change, but occuring six months earlier. The start epoch of the transition in phase corresponds to the yellow square in Figure 4. Note that the green transition revolutions are higher in this case since the ecliptic angle of the Moon is positive. In fact, a three-hour eclipse is encountered along one of the transition revolutions. The OM burn magnitudes for the successful, eclipse-free transition are plotted in Figure 20(a). Note that before and after the phase change, the stationkeeping burn magnitude is of nominal magnitude (see Figure 14(a) and 15(a)). The maneuvers associated with the phase change revolutions are significantly larger, reaching up to approximately 1.2 m/s on some revolutions. The cumulative maneuver cost is plotted in Figure 20(b). The phase change alone requires approximately 17.5 m/s over 6 months. Figure 20(c) contains two curves. The blue curve corresponds to the perilune passage time of the spacecraft measured relative to the nominal baseline. The changing of phase over the revolutions is evident, as is the maintenance of the spacecraft at a shifted phase after revolution 98. The red curve corresponds to the perilune passage time error as measured relative to the targeted perilune passage time. During the phase change maneuver, the error in achieved perilune passage time is slightly larger than the error observed when performing nominal OM in either eclipse-avoidant phase. Finally, the position errors in the inertial frame measured relative to the position values along the targeted baseline are plotted in Figure 20(d). Similar to the red curve in Figure 20(c), errors are larger during the transition revolutions, but return to a nominal magnitude once in the alternative eclipse-avoidant baseline.

Figure 21 illustrates osculating orbital parameters computed at perilune of each revolution of the trajectory depicted in Figure 19(a). The circularizing of the transition revolutions during the phase change is apparent as the trend in perilune radius (see Figure 21(a)) increases and eccentricity (see Figure 21(b)) decreases. The orbital period of the transition revolutions is larger during the phase change than it is during revolutions in the nominal and alternative eclipse-avoidant phases, as is depicted in Figure 21(c).

CONCLUDING REMARKS

A strategy to rapidly and autonomously compute many-revolution baseline trajectories is developed and is demonstrated to produce a 20 year 9:2 NRHO baseline in the nominal Gateway phase. OM performed on a spacecraft targeting states obtained from this new baseline is demonstrated to be nearly identical to OM performed based on targets obtained from the original 2017 Gateway baseline. Numerical challenges associated with producing such large ballistic trajectories are addressed and managed to develop an algorithm that requires relatively little wall time to run. Geometric properties associated with eclipse avoidance while maintaining a spacecraft in a baseline NRHO or while transitioning between phases along an NRHO are presented. Finally, an OM-based phase change strategy is used to successfully avoid an eclipse along a baseline and to transition between the two eclipse-avoidant phases of the 9:2 NRHO while avoiding eclipses during the transition.

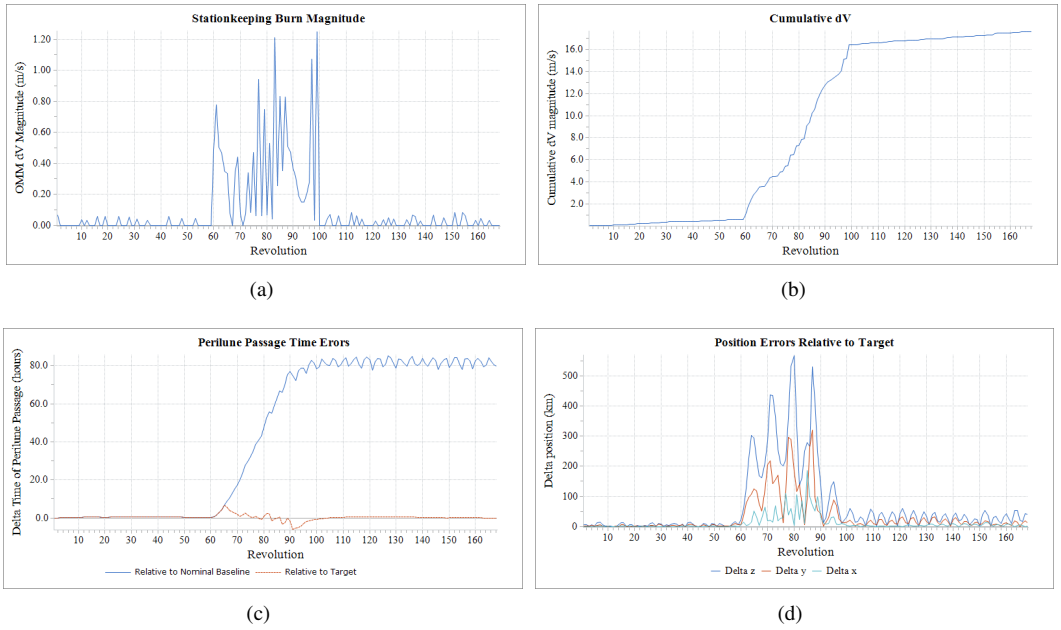

Figure 20. Half-period phase change from one eclipse-avoidant phase of the 9:2 NRHO to the other

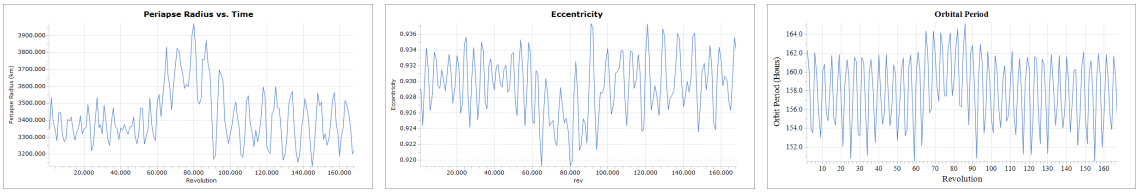

Figure 21. Osculating orbital parameters measured over the phase change depicted in Figure 19(a)

ACKNOWLEDGMENTS

The authors wish to thank Dave Lee at NASA Johnson Space Center for his insight into NRHO baseline generation and significant contribution to the original baseline generation effort.

REFERENCES

[1] M. Gates, M. Barrett, J. Caram, V. Crable, D. Irimies, D. Ludban, D. Manzell, and R. Ticker, "Gateway Power and Proulsion Element Development Status," *67th International Astronautical Congress*, Bremen, Germany, October 2018.

[2] D. E. Lee, "White Paper: Gateway Destination Orbit Model: A Continuous 15 Year NRHO Reference Trajectory," Tech. Rep. Document ID: 20190030294, National Aeronautics and Space Administration, NASA Johnson Space Center, Houston, TX, August 20 2019.

[3] D. C. Davis, S. T. Scheuerle, D. A. Williams, F. S. Miguel, E. M. Zimovan-Spreen, and K. C. Howell, "Orbit Maintenance Burn Details for Spacecraft in a Near Rectilinear Halo Orbit," *AAS/AIAA Astrodynamics Specialist Conference*, Charlotte, NC, August 2022.

[4] D. E. Lee, R. J. Whitley, and C. Acton, "Sample Deep Space Gateway Orbit," `https://naif.jpl.nasa.gov/pub/naif/misc/MORE_PROJECTS/DSG/`, July 2018. NAIF Plantary Data System Navigation Node, NASA Jet Propulsion Laboratory.

[5] D. C. Davis, E. M. Zimovan-Spreen, S. T. Scheuerle, and K. C. Howell, "Debris Avoidance and Phase Change Maneuvers in Near Rectilinear Halo Orbits," *44th Annual AAS Guidance, Navigation, and Control Conference*, Breckenridge, CO, February 2022.

[6] B. McCarthy, E. Zimovan-Spreen, D. Davis, S. Scheuerle, and K. Howell, "Rephasing and Loitering Strategies in the Gateway Near Rectilinear Halo Orbit," *AAS/AIAA Astrodynamics Specialist Conference*, Big Sky, MT, August 13-17 2023.

[7] a.i. solutions, Inc., "Freeflyer Version 7.6.1," 2021.

[8] E. M. Z. Spreen, *Trajectory Design and Targeting for Applications to the Exploration Program in Cislunar Space*. PhD thesis, Purdue University, 2021.

[9] D. C. Davis, F. S. Khoury, K. C. Howell, and D. J. Sweeney, "Phase Control and Eclipse Avoidance in Near Rectilinear Halo Orbits," *AAS Guidance, Navigation and Control Conference,*, Breckenridge, CO, January 30 - February 5 2020.

[10] J. Williams, D. E. Lee, R. J. Whitley, K. A. Bokelmann, D. C. Davis, and C. F. Berry, "Targeting Cislunar Near Rectilinear Halo Orbits for Human Space Exploration," *AAS/AIAA Space Flight Mechanics Meeting*, San Antonio, TX, February 5 2017.

[11] "Numerical Integration," `https://www.gnu.org/software/gsl/doc/html/integration.html`. GNU Scientific Library.

[12] "mldivide," `https://www.mathworks.com/help/matlab/ref/mldivide.html`. Mathworks Help Center.

[13] E. Howell, "Blue Origin will build NASA's new moon lander for Artemis astronauts," `https://www.space.com/nasa-selects-blue-origin-second-artemis-moon-lander`, May 19 2023.

[14] J. Foust, "NASA selects Blue Origin to develop second Artemis lunar lander," `https://spacenews.com/nasa-selects-blue-origin-to-develop-second-artemis-lunar-lander/`, May 19 2023.